Conformation of Fork Junction DNA in a Complex with *Escherichia coli* RNA Polymerase†

Ewa Heyduk and Tomasz Heyduk*

Edward A. Doisy Department of Biochemistry and Molecular Biology, St. Louis University Medical School, 1402 South Grand Boulevard, St. Louis, Missouri 63104

Received December 10, 2001

ABSTRACT: *Escherichia coli* RNA polymerase is able to bind fork junction DNA containing a conserved −10 promoter element in a sequence-specific manner, and it is believed that polymerase−fork junction DNA interaction mimics those between the enzyme and the promoter DNA in the open complex. In this report we determined the conformation of polymerase-bound fork junction DNA in solution. A series of distances between sites in the fork junction DNA in complex with polymerase were determined using luminescence and fluorescence resonance energy transfer. A series of fork junction DNAs were prepared containing the luminescent or fluorescent donor probe at the upstream or at the downstream end of the fork DNA and acceptor probes at nine positions within the fork junction DNA. The measured distances were compared with analogous distances in a model reference DNA duplex, and the observed distance differences were used to build a model of the fork junction DNA in a complex with the polymerase. The obtained model revealed an insignificant perturbation of the duplex part of the fork DNA in a complex with the polymerase whereas a sharp kink of DNA was observed at the ds/ss DNA boundary of the fork junction DNA.

Transcription initiation involves two major steps: promoter DNA recognition and promoter DNA melting to form a complex capable of template-directed synthesis of mRNA (*1*). In bacteria, transcription is carried out by a multisubunit RNA polymerase. Recent years brought significant advancements in understanding of the molecular events leading to transcription initiation (for recent reviews, see refs *2*−*6*). An important aspect of such understanding is to learn about the structure of RNA polymerase and its complexes with promoter DNA at various intermediate states of transcription initiation reaction. This is a daunting task due to the complexity and the size of these complexes. The progress in this regard was very significant in recent years. The crystallographic or NMR[1] structures of various subunits of bacterial RNA polymerase or their domains have been determined (*7*−*9*). The low-resolution electron microscopy images of the enzyme were obtained (*10*−*12*), and low-resolution images of RNA polymerase−promoter complexes were collected using atomic force microscopy (*13*). Finally, the crystal structure of the core enzyme from *Thermus aquaticus* was determined, which provided the most detailed insight into the structure of the bacterial enzyme (*14*). The availability of the crystal structure of the core enzyme allows now structural interpretation of the results from other indirect approaches and will also provide necessary background information for the attempts of molecular modeling of other forms and complexes of the enzyme.

In this work we present the results of solution structural measurements on a model fork junction DNA in complex with RNA polymerase holoenzyme. It was shown previously that RNA polymerase recognizes fork junction DNA containing conserved −10 and −35 promoter sequence elements in a sequence-specific manner (*15*−*17*). Thus, a complex of RNA polymerase holoenzyme with the fork junction DNA constitutes the simplest model for RNA polymerase−promoter DNA interactions in the open complex. We prepared a series of fork junction DNAs with a luminescent (or fluorescent) donor at either upstream or downstream end of the molecule and with fluorescent acceptor molecules incorporated into nine positions within DNA. The luminescence resonance energy transfer (LRET) (*18*−*20*) and fluorescence resonance energy transfer (FRET) (*21*−*22*) measurements were then used to determine distances between the probes. Both energy transfer techniques allow measurement of atomic scale distances in solution under biologically relevant conditions. LRET is a variant of the FRET in which long-lived lanthanide chelate probes are used, which simplifies distance determination and eliminates uncertainty of the measurement due to the relative orientation of the donor and acceptor probes (*18*−*20*). The measured distances were used to build a structural model of the DNA. The holenzyme-bound fork junction DNA appears to be sharply kinked at the ds/ss DNA junction, suggesting that the trajectory of promoter DNA in the open complex exhibits an abrupt change at the ds/ss junction.

† This work was supported by NIH Grant GM50514.

* Corresponding author. E-mail: heydukt@slu.edu. Fax: (314) 577-8156. Phone: (314) 577-8152.

[1] Abbreviations: NMR, nuclear magnetic resonance; ss, single stranded; ds, double stranded; FRET, fluorescence resonance energy transfer; LRET, luminescence resonance energy transfer; DTPA, diethylenetriaminepentaacetic acid; AMCA, 7-amino-4-methyl-3-coumarinylacetic acid; CPM, 7-(diethylamino)-3-(4′-maleimidylphenyl)-4-methylcoumarin; RNAP, RNA polymerase.

10.1021/bi012133i CCC: $22.00
Published on Web 01/31/2002

MATERIALS AND METHODS

Materials. Cy5 and Cy3 monosuccinimidyl esters (*23*) were purchased from Amersham Pharmacia Biotech (Piscataway, NJ), and CPM was purchased from Molecular Probes (Eugene, OR). Diethylenetriaminepentaacetic acid−7-amino-4-methylcoumarin maleimide (DTPA−AMCA-maleimide) was prepared in our laboratory as previously described (*24*). The reagents for oligonucleotide synthesis were purchased from Glen Research (Sterling, VA). The amine-VN phosphoramidite used to incorporate the reactive amine into the oligonucleotides was from Clontech (Palo Alto, CA). RNA polymerase was purified from *Escherichia coli* K12 cells (University of Alabama fermentation facility) using the method of Burgess and Jendrisak (*25*) as modified by Polyakov et al. (*26*) and Hager et al. (*27*). $EuCl_3$ and D_2O were from Sigma (St. Louis, MO). All the other reagents were of the highest purity commercially available.

Oligonucleotides. The oligonucleotides used for this study were synthesized on an Applied Biosystems model 394 DNA synthesizer (Foster City, CA) using standard phosphoramidate chemistry. Oligonucleotides were synthesized in trityl-on form and were subsequently purified on a PRP-1 reverse-phase column (Hamilton, Reno, NV). The amine-VN-containing oligonucleotides were labeled with Cy5 (or Cy3) by incubation of 20−30 nmol of oligonucleotide with 1−2 mM Cy5 (or Cy3) monosuccinimidyl ester for ~18 h at room temperature. Following the reaction, the excess of unreacted Cy5 (or Cy3) label was removed on a G-25 spin column (Pharmacia-Amersham), and the labeled oligonucleotides were further purified on a 1 mL RPC reverse-phase column (Pharmacia-Amersham). The oligonucleotides labeled at the 5′ or the 3′ end with DTPA−AMCA-maleimide were prepared by first converting the 5′-phosphate or 3′-phosphate to a cystamine derivative (*28*). The cystamine derivative, after reduction with 1 mM DTT, was reacted with 2 mM DTPA−AMCA-maleimide in 20 mM Tris-HCl (pH 8.0), 100 mM NaCl, and 10 μM EDTA buffer for 4 h at room temperature. The excess of the chelate was removed on a G-25 spin column (Amersham Pharmacia Biotech), and the modified oligonucleotide was purified on a 9 × 250 mm DNAPAC PA-100 column (DIONEX, Sunnyvale, CA). A convex gradient of 37−62% of buffer B was used, and the column was run at 4 mL/min. Buffer A: 25 mM Tris-HCl (pH 8.0) and 10 μM EDTA. Buffer B: buffer A + 1 M NaCl. Fractions containing the correct product (as confirmed by MALDI mass spectrometry) were pooled, and 10 μM $EuCl_3$ was added. After 30 min of incubation at room temperature the excess of $EuCl_3$ and the salt were removed on a Sep-Pak C18 cartridge (Waters). The modified oligonucleotide was eluted with 50% acetonitrile and was dried in a Speed-Vac. DNA duplexes were formed by mixing equimolar amounts of appropriate complementary strands in 20 mM Tris-HCl (pH 8.0) buffer containing 100 mM NaCl and 10 μM EDTA, followed by heating for 1 min at 95 °C and cooling to room temperature in 2 h. Fluorescein at the 3′ end of the nontemplate strand was incorporated during oligonucleotide synthesis and was purified by reverse-phase HPLC as described previously (*29*).

Electrophoretic Mobility Shift Assays. Resistance of polymerase−fork junction DNA complexes to heparin challenge was determined using electrophoretic mobility shift assay (*15*). RNAP (80 nM) was incubated for 30 min on ice with a Cy5-labeled fork junction DNA (40 nM) in 20 mM Tris-HCl (pH 8.0) buffer containing 100 mM NaCl, 10 μM EDTA, 5 mM $MgCl_2$, 5% glycerol, 0.1 mM DTT, and 50 μg/ mL albumin. Heparin (100 μg/mL) was added to the mixture, and the samples were incubated for 1 min on ice and were loaded on 7.5% native polyacrylamide gel. The gel was run in 1× TBE buffer, and DNA bands were visualized by scanning with STORM (Molecular Dynamics, Sunnyvale, CA), detecting fluorescence of Cy5-labeled DNA.

Luminescence Resonance Energy Transfer Measurements. LRET experiments were performed in a 120 μL cuvette on a laboratory-built two-channel instrument described earlier (*29, 30*). Reaction mixtures contained 50 nM polymerase and 25 nM fork junction DNA in 20 mM Tris-HCl (pH 8.0) buffer containing 100 mM NaCl, 10 μM EDTA, 5 mM $MgCl_2$, 5% glycerol, 0.1 mM DTT, and 50 μg/mL albumin. Reaction mixtures were incubated for 5 min at 25° C before the luminescence lifetime measurement was performed. The donor emission was collected using a 620 nm interference filter (Oriel, Stratford, CT) whereas the sensitized acceptor signal was detected using a 668 nm interference filter (Oriel, Stratford, CT). The decay curves were analyzed by nonlinear regression using SCIENTIST (Micromath Scientific Software, Salt Lake City, UT) according to

$$I = \sum I_i \exp(-t/\tau_i) + B \quad (1)$$

where I_i and t_i are the amplitude and the lifetime of the ith component and B is the background noise. Energy transfer was calculated using (*21, 22*)

$$E = 1 - \tau_{DA}/\tau_D \quad (2)$$

where τ_{DA} and τ_D are luminescence lifetimes of the donor in the presence and absence of the acceptor, respectively. The distances between donor and acceptor were calculated according to (*21*)

$$R^6 = R^6_o(1 - E)/E \quad (3)$$

where R is a distance between a donor and an acceptor and R_o is a distance at which the energy transfer is 0.5. The R_o for (Eu^{3+})DTPA−AMCA and the Cy5 donor−acceptor pair (55 Å) was calculated as described previously (*29*). In calculating R_o, a completely randomized orientation of donor and acceptor fluorochromes was assumed (*18−20, 29*). For calculating distances measured in a buffer containing D_2O, the R_o values were calculated as described previously (*29*) using the quantum yield of the donor calculated according to

$$q_d = \tau_d/\tau_{d(100\%)} \quad (4)$$

where τ_d is a lifetime of the donor in a water/D_2O mixture and $\tau_{d(100\%)}$ is a lifetime in 100% D_2O.

All distances reported in Tables 1, 2, and 4 are averages from two to six measurements. The error of measured distances calculated as standard error of the mean of independent measurements was less then 3%. However, this error is likely to be a low estimate of the true error since it does not include uncertainties inherent to the energy transfer technique (for example, uncertainty of orientation factor).

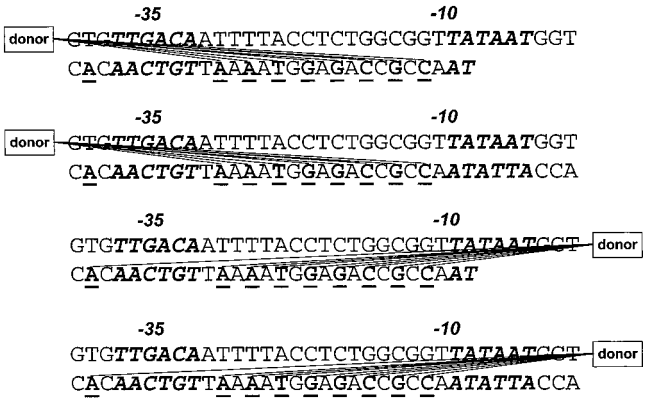

FIGURE 1: Fork DNA and reference duplex DNA used in LRET and FRET measurements. The −35 and −10 sequences are in italic bold type. Positions where Cy5 and Cy3 acceptors were incorporated are in bold type and are underlined.

FRET and Time-Dependent Anisotropy Measurements. Nanosecond decays of CPM and fluorescein were measured using time-correlated single photon counting (TCSPC) (*31*). The excitation in the case of CPM was at 405 nm with a pulsed diode laser (IBH, Glasgow, Scotland) operating at 1 MHz, and the emission was collected with a 520 nm interference filter. The excitation in the case of fluorescein was at 480 nm [using a 480 nm interfernce filter and a 495 nm pulsed LED (IBH, Glasgow, Scotland)], and the emission was collected with a 520 nm interference filter. Fluorescence was detected by an integrated detection module (TBX-04, IBH) containing a photomultiplier, preamplifier, and constant-fraction discriminator. The output from this module was processed by time-correlated single photon counting. The instrument response function measured with a LUDOX suspension (DuPont) had a full width at half-maximum of 250 ps (405 nm excitation) and 1.2 ns (480 nm excitation). Decays were fitted to a sum of exponentials using the standard deconvolution procedure (*32*). Energy transfer calculations were performed according to eqs 2 and 3 using number-averaged lifetimes. All intensity decays were recorded with the excitation and emission polarizers at "magic angles". Time-dependent anisotropy decays were measured with the excitation polarizer set at vertical orientation, and the emission polarizer was cycled during data acquisition between vertical and horizontal orientation by a computer-controlled motorized accessory. Time-dependent anisotropy decays were quantitatively analyzed by the impulse reconvolution method (*33*) using software from IBH.

RESULTS

The major goal of this work was to obtain a model of the conformation of the fork junction DNA bound to RNA polymerase holoenzyme. This DNA molecule mimics interactions between the polymerase and promoter DNA in the open complex, providing a simple model for structural and thermodynamic studies. The approach taken in this work was to prepare a series of fork junction DNA containing luminescent (or fluorescent) donor and fluorescent acceptor at different locations within DNA molecule (Figure 1). The donor was incorporated at the 5′ end or the 3′ end of the top (nontemplate) strand. The acceptor was incorporated into nine different locations in the bottom strand. Eight sites were in the spacer region between the −10 and −35 sequences, and one site was in the upstream −35 region. Thus, in principle a total of 17 distances between a total of 11 positions within the fork DNA could be measured using this set of DNA molecules. One distance (between the donor at the 5′ end of the top strand and acceptor at position −37) could not be measured since the probes were too close to each other. Determination of an overall architecture of a reasonably large molecule from energy transfer distance measurements is a difficult task. Very rarely will it be possible to determine enough distances to allow unambiguous placement of many (in this case 11) points in three dimensions. To simplify this task, we decided to use a reference molecule of known conformation [full duplex analogue of the fork DNA (Figure 1)] and to compare the distances between donor and acceptor probes within the fork DNA bound to the holoenzyme with the distances between identical sites within the reference duplex DNA. Differences in distances (which are easier to measure by energy transfer then the actual distances) between these two molecules could be then used to conclude about the deviation of the fork DNA from the structure of the reference duplex.

Fluorescence acceptors were introduced into the DNA by a covalent modification of the abasic analogue containing a reactive aliphatic amino group attached to the sugar backbone (Figure 2C). We have determined if this mode of fluorochrome incorporation did not inhibit the ability of polymerase to bind fork DNA in a sequence-specific manner. The ability of polymerase holoenzyme to bind acceptor-labeled fork junction DNAs was tested using electrophoretic mobility shift assay (Figure 2A). The results show that essentially 100% of DNA was bound under conditions of a small molar excess of polymerase. Figure 2 also shows that the complexes formed exhibited resistance to the challenge with heparin, a hallmark of a sequence-specific recognition of fork junction DNA (*15*). We concluded that labeling of internal sites in the fork junction DNA did not adversely affect interaction of this DNA with polymerase. Further control experiments showed that the binding of labeled fork junction DNA under our experimental conditions was sequence specific. Formation of a complex of RNA polymerase with Cy5-labeled fork junction DNA was inhibited efficiently in the presence of the unlabled consensus sequence fork junction DNA whereas a fork junction DNA in which −10 and −35 DNA sequences were eliminated was a poor competitor (Figure 2B). Solution fluorescence binding experiments (not shown) revealed that the equilibrium dissociation constant for the labeled fork junction DNA−polymerase complex was ∼10 nM. Thus, all subsequent experiments were performed with the polymerase at 50 nM concentration, ensuring ∼100% saturation of DNA with the polymerase.

We first determined the conformation of the duplex part of the fork DNA in complex with polymerase. The 5′ end of the top strand of the reference duplex and the fork DNA was labeled with the (Eu^{3+})DTPA−AMCA (donor), and the eight positions within the spacer region were labeled with Cy5. Distances between these positions were determined by LRET. Figure 3 shows typical examples of luminescence decay curves obtained in these experiments. Figure 3A shows that a donor-only labeled sample (the donor at the 5′ end of the top strand) decayed in a single-exponential manner. The example of donor decay in the donor−acceptor-labeled sample (donor at the 5′ end of the top strand and the acceptor

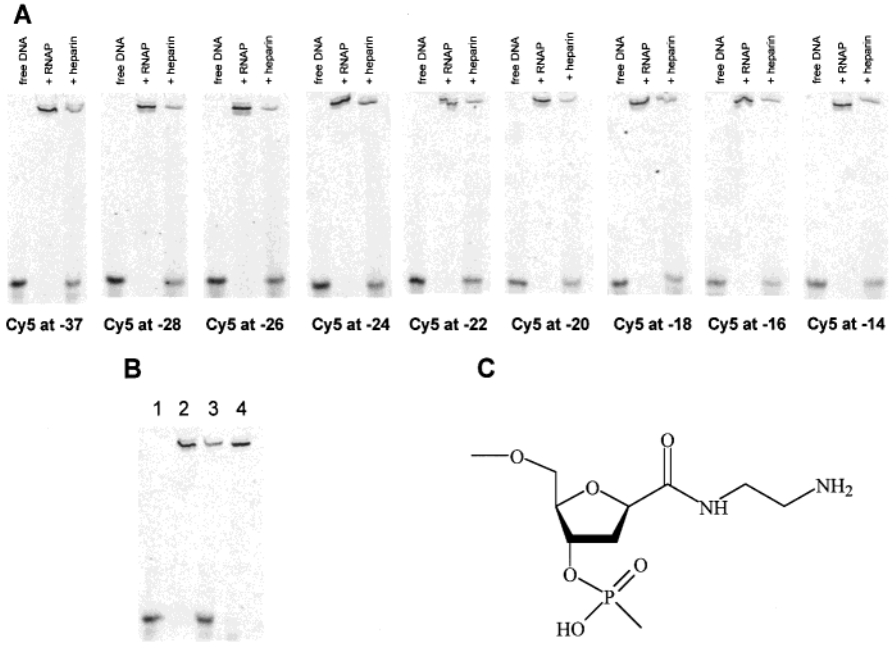

FIGURE 2: (A) Binding of acceptor-labeled fork junction DNAs to RNA polymerase. Cy5-labeled fork DNAs were used. Formation of the polymerase−DNA complex was detected by electrophoretic mobility shift assay (*14*). The lanes labeled free DNA contained Cy5-labeled fork junction DNA only, the lanes labeled +RNAP contained Cy5-labeled fork junction DNA and RNA polymerase, and the lanes labeled +heparin contained Cy5-labeled fork junction DNA incubated with RNA polymerase followed by addition of heparin. (B) Sequence specificity of polymerase−fork junction DNA complex formation. Binding of Cy5-labeled fork junction DNA to RNA polymerase in the presence of a 10-fold excess of unlabeled fork junction DNA (lane 3) and a 10-fold excess of unlabeled fork junction DNA in which −10 and −35 consensus hexamers were replaced by unrelated sequences (lane 4) is compared. Lane 1 is Cy5-labeled fork junction DNA in the absence of polymerase, and lane 2 is the binding experiment in the absence of the competitor. (C) Structure of amine-VN (Clontech, Palo Alto, CA) used to incorporate acceptors into internal sites of DNA.

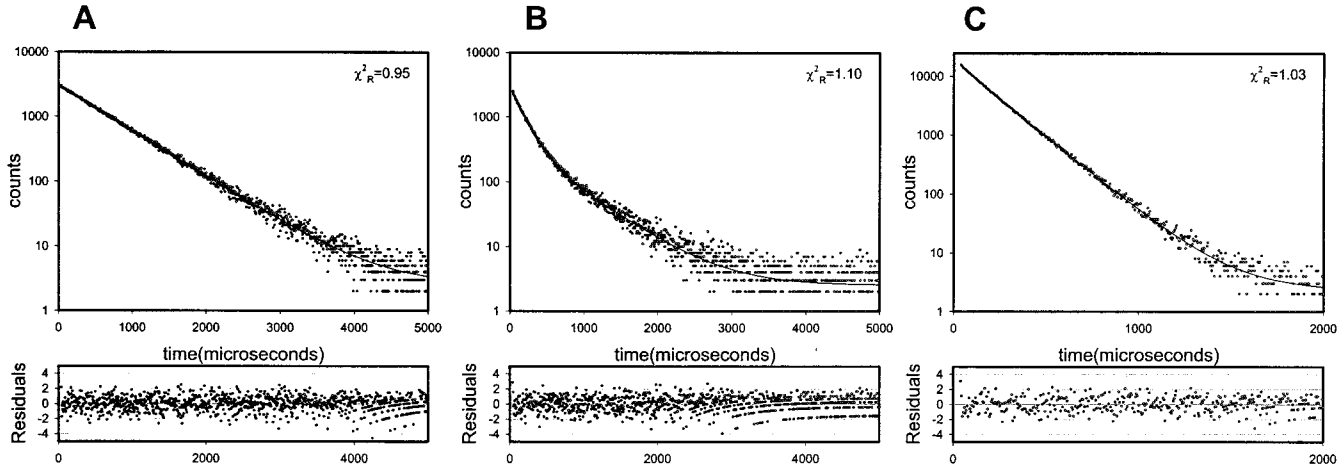

FIGURE 3: Luminescence decays of fork junction DNA in complex with RNA polymerase. (A) Decay of the donor-only sample; (B) donor decay in the donor−acceptor-labeled sample; (C) sensitized acceptor decay in the donor−acceptor-labeled sample. Solid lines represent the best fit to a single-exponential equation (A) or double-exponential equation (B and C). The data shown are for a sample with the donor at the 5′ end of the top strand and with the acceptor at position −23.

at −23 position on the bottom strand) is shown in Figure 3B. The decay of the donor in this case required fitting to a double-exponential decay function (Figure 3B). The major component (86%) decayed with a lifetime (158 μs) which was much shorter than the lifetime observed for the donor-only sample (615 μs) whereas the minor component (13%) decayed with a lifetime (563 μs) similar to the lifetime of the unquenched donor. Thus, the major decay component corresponded to the donor engaged in energy transfer with the acceptor whereas the minor component represented the population of donors unable to transfer energy due to incomplete labeling or incomplete annealing of the DNA molecule. This interpretation is consistent with the sensitized acceptor decay data (Figure 3C). The sensitized acceptor signal in the case of the europium chelate−Cy5 donor−acceptor pair can only be observed if the acceptor is excited via energy transfer from the donor (*18*−*20*, *29*). The decay of the sensitized acceptor signal was fitted to a double-exponential decay equation (Figure 3C). The lifetime (173 μs) of the major component (82%) was very similar to the lifetime of the major component in donor decay observed in the same sample (Figure 3B). The minor component decayed with a lifetime of 83 μs. Interpretation of the amplitudes of sensitized acceptor decays should take into account the fact that they do not represent properly populations of donors from which different components of sensi-

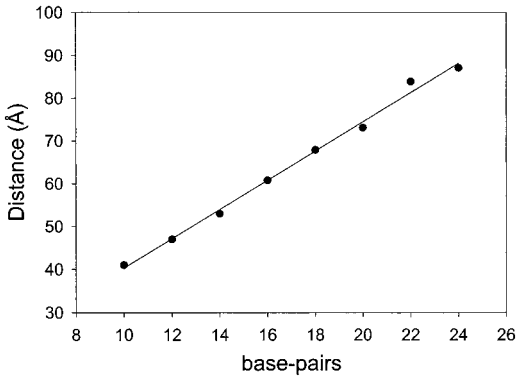

FIGURE 4: Relationship between the donor−acceptor distance determined by LRET and the number of base pairs separating them in reference duplex DNA. The solid line is a linear regression line (correlation coefficient of 0.997).

Table 1: Summary of LRET Distance Measurements with the Donor at the 5′ End of the Nontemplate Strand (Position −38)

	distance (Å)			
acceptor position	in full reference duplex	in fork	in fork + holoenzyme	Δ [(fork + holoenzyme)− full duplex] (Å)
−28	41.0	40.5	39.3	−1.7
−26	47.0	47.0	46.7	−0.3
−24	53.0	53.4	52.7	−0.3
−22	60.8	62.0		
−20	67.9	69.3		
−18	73.1	75.3	75.7	+2.6
−16	83.9	84.3	80.9	−3.0
−14	87.1	89.2	85.8	−1.3

tized acceptor decay arise (*30*). This is because the amplitude of sensitized acceptor decay depends not only on the concentration of donors but also on the rate constant of energy transfer (*30*). When the amplitudes of the two components in sensitized acceptor decay were corrected for this effect as described previously (*30*), it appeared that the amplitude of the major component was even higher (92%). Thus, in all subsequent analyses only this major component was taken into consideration. The minor fast-decaying component was observed with all DNAs used in this study and was always <10%. The simplest interpretation of this minor component is that it corresponded to some nonspecific aggregates. Also, in all subsequent analyses only the sensitized acceptor decays were used since, compared to donor decays, they allow more accurate determinations of τ_{da}. This is especially true when the energy transfer is low. Under these conditions it is difficult to determine τ_{da} because its value becomes close to the value of τ_d and donor decays always contain a small component corresponding to the unquenched donor. Some of these distance measurements were repeated in a buffer containing 75% D_2O. Under these conditions the quantum yield and the lifetime of europium chelate are increased, resulting in a larger value of R_o (*19*, *20*, *29*). This provides a more stringent test for the reproducibility of measured distances and allows a more precise measurement of longer distances. Table 1 summarizes distances calculated from these LRET experiments. In the case of reference duplex DNA there was a simple linear dependence of the measured distance on the number of base pairs separating the donor and acceptor (Figure 4). A straight line could adequately represent experimental data with a correlation coefficient of 0.997, and the slope was 3.4 ± 0.1 Å/bp (identical to an axial rise of the B-DNA duplex). Clegg et al. (*34*) have shown that relative positions of donor and acceptor molecules with regard to the axis of DNA can be determined by studying the energy transfer between the donor and the acceptor in a series of model DNA duplexes in which the number of base pairs separating the labels is varied in a systematic way. This approach is based on the observation that for donors and acceptors located on the axis of the DNA duplex a simple linear dependence of the distance on the number of base pairs separating the donor and acceptor should be observed. However, for donor and acceptors which are located at some distance from the axis, the helical periodicity of the distance should be observed and the dependence of the distance on the number of base pairs separating the donor and acceptor should be nonlinear. A simple linear dependence of the measured distance on the number of base pairs separating the donor and acceptor observed for the reference duplex suggested that donor and acceptor labels were collinear with the long axis of the DNA duplex and indicated that distances measured with this donor−acceptor pair reflect the DNA duplex backbone conformation. This simple collinear localization of the donor and acceptor is very likely due to the method of attachment of acceptors to the DNA employed in this work. The acceptors were covalently attached to an aliphatic amino group located on the sugar residue of DNA backbone (Figure 2C). Thus, the acceptor effectively replaced the base at the point of attachment to the DNA backbone, and thus it is likely that the fluorophore was held near the axis of the duplex through stacking interactions to neighboring base pairs. It was found previously that Cy3, a fluorochrome very similar in structure to the Cy5 used as an acceptor in our LRET experiments, was stacked on the terminal base pair when attached to the 5′ end of the DNA duplex (*35*).

Analogous distances in the fork DNA and in the fork DNA in complex with the holoenzyme were very similar (Table 1). The distances to the acceptor at positions −20 and −22 of the bottom strand were not used in the case of fork DNA bound to the holoenzyme because sensitized acceptor decays for this DNA could not be fitted to simple models illustrated by Figure 3 (not shown), suggesting that the label at position −20 or −22 perturbed the DNA−polymerase complex. Distance differences measured between the fork bound to the holoenzyme and the reference duplex were small, and most of them were negative. The simplest interpretation of these results is that the conformation of the duplex part of the fork DNA was not perturbed greatly upon binding to the polymerase.

To obtain information regarding the conformation of the ss part of the fork DNA, the 3′ end of the top strand of the reference duplex and the fork DNA was labeled with the (Eu^{3+})DTPA−AMCA (donor) and the eight positions within the spacer region and one position upstream of the −35 hexamer were labeled with Cy5 (Table 2). In the case of the reference duplex, distances to positions −28 and −37 could not be measured since at these long donor−acceptor distances we were unable to obtain good quality LRET data. In the case of fork DNA alone, distances to positions −14 and −16 could not be measured since apparently donor−acceptor distances in these cases were too short for good quality decay measurements. In the case of fork DNA in the presence of

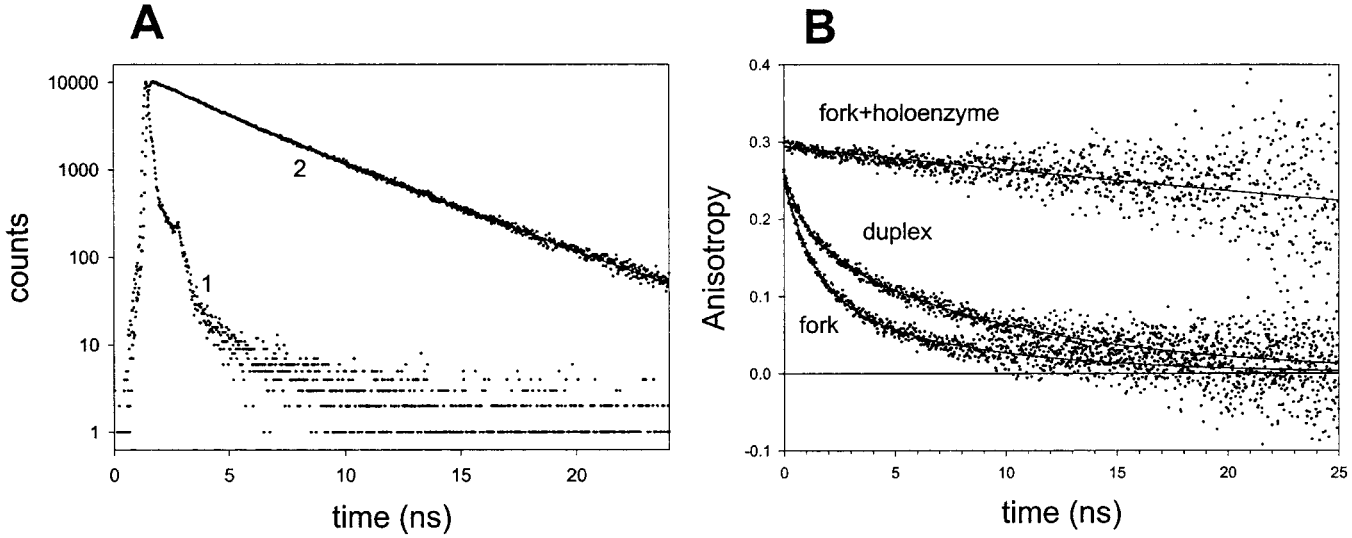

FIGURE 5: Time-dependent anisotropy decays of fork DNA labeled at the 3′ end of the top strand with CPM. (A) Time-dependent intensity decay of fork DNA at magic angles (curve 2). The solid line represents the best fit of the data to a double-exponential decay equation. The resolved lifetimes were 1.49 ns (0.33 amplitude) and 4.17 ns (0.67 amplitude). The pulse profile is also shown (curve 1). (B) Time-dependent anisotropy decays for free fork DNA, fork DNA in complex with the holoenzyme, and duplex DNA. Solid lines are fits to double-exponential decay (fork and duplex) and single-exponential decay (fork + holoenzyme). The anisotropy decay parameters were obtained by impulse reconvolution analysis (*33*) and are summarized in Table 3.

Table 2: Summary of LRET Distance Measurements with the Donor at the 3′ End of the Nontemplate Strand (Position −4)

	distance (Å)			
acceptor position	in full reference duplex	in fork	in fork + holoenzyme	Δ [(fork + holoenzyme)− full duplex] (Å)
−14	36.0		33.7	−2.3
−16	39.5		39.3	−0.2
−18	56.3	41.3	42.5	−13.8
−20	63.5	39.1		
−22	67.4	41.8		
−24	73.7	46.9	53.8	−19.9
−26	78.9	49.6	68.4	−10.5
−28		61.6	70.8	
−37		85.6	100.9	

Table 3: Summary of the Analysis of Time-Resolved Fluorescence Polarization Experiments

sample	Φ_1 (ns)[a]	A_1[a]	Φ_2 (ns)[a]	A_2[a]
fork	0.7	0.150	5.0	0.147
duplex	0.8	0.089	9.3	0.182
fork + holoenzyme	∼90[b]	0.295		

[a] Apparent rotation correlation times and amplitudes obtained by impulse reconvolution analysis of time-dependent anisotropy data. [b] This is a poorly defined value since very little anisotropy decay occurred within the observation time allowed by the lifetime of the excited state of the probe (Figure 5B).

polymerase distances to positions −20 and −22 were not measured since, as described above, sensitized acceptor decays for this DNA could not be fitted to simple models illustrated by Figure 3. Also, the distance to position −37 was not measured because the distance was too long. Comparison of analogous distances obtained with the fork DNA alone and the duplex revealed that the distances in the case of fork were much smaller. In the presence of the holoenzyme, the distances were increased, and the comparison with the reference duplex DNA revealed that the short-range distances (to the sites adjacent to the −10 hexamer) were very similar in fork DNA bound to the holoenzyme and in the reference duplex. In contrast, long-range distances (to the sites adjacent to the −35 hexamer) were significantly shorter in the case of fork bound to RNAP (Table 2). The interpretation of the LRET data in the case of the donor located in the ss fork extension requires considering a possible effect of the flexibility of the single-stranded extension of the fork. In contrast to the rigid DNA duplex, single-stranded extension of the fork DNA could undergo flexible movements. The lifetime of the donor used in LRET experiments is in the microsecond range, which should provide enough time for the flexible ss tail to assume all possible transient positions. Thus, the distance measured by LRET under these conditions would correspond to the distance of the closest approach between the donor and acceptor and would not report an average distance. To directly address potential flexibility of the ss tail in the fork DNA, time-resolved fluorescence anisotropy measurements were performed. The 3′ end of the top strand of the fork DNA was labeled with CPM. The decay of the probe in fork alone was double exponential (Figure 5A) with the majority of fluorescence decaying with a lifetime of ∼4 ns. Intensity decay in the presence of RNAP was also double exponential, and the decay parameters were only slightly different from those observed for fork DNA alone (not shown). Figure 5B shows anisotropy decays for the fork in the presence and absence of RNAP and for the reference duplex DNA. Visual inspection of the curves and quantitative analysis of anisotropy decay parameters (Table 3) revealed evidence for a significant flexibility of the ss tail in the fork DNA in the absence of polymerase. The anisotropy decay of the fork alone was much faster compared to the full duplex. The mass difference between the fork and the duplex DNA is only ∼10%, which would produce an insignificant difference in the anisotropy decay parameters between the fork and the duplex. Thus, the large observed difference between the anisotropy decays of fork and duplex DNA was entirely due to the flexibility of the ss tail in the fork. In the presence of RNA polymerase anisotropy decay was very slow, reflecting

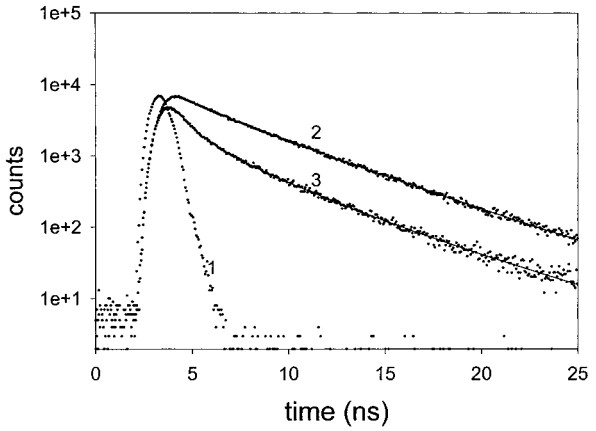

FIGURE 6: Examples of intensity decay data for the DNA labeled at the 3′ end of the top strand with fluorescein. Decays were recorded at magic angles. Curves: 1, pulse profile; 2, donor-only decay; 3, donor−acceptor labeled with the acceptor at position −14. Solid lines correspond to the fits to double-exponential decay equations. The resolved decay lifetimes for donor-only samples were 1.64 ns (32% amplitude) and 4.63 ns (68% amplitude). The resolved decay lifetimes for the donor−acceptor sample were 0.47 ns (77% amplitude) and 1.98 ns (23% amplitude). When fitting donor−acceptor decays, a fixed 10% component with 4.63 ns lifetime was included since all donor−acceptor decay had ∼10% unquenched donor component likely due to incomplete labeling or incomplete DNA hybridization.

tumbling of the entire complex. No evidence for local flexibility of the fork DNA within the complex was evident since the anisotropy decay could be well described by a single rotation correlation time (Table 3). We concluded that in the complex with RNAP fork DNA is rigidly bound to the enzyme and thus in this case LRET distances would correctly report the overall conformation of the fork DNA. Comparing these distances with the distances measured in the reference duplex could be used to conclude about the conformation of the ss tail of the fork in complex with RNAP. In contrast, for the fork alone the flexibility of the ss tail prohibits the use of LRET data to conclude about the "average" conformation of the molecule. The surprisingly short distances found in the fork alone were due to the ability of the donor to transiently come into close proximity of acceptors due to flexible movements of the tail during the long excited-state lifetime of the donor.

To obtain independent confirmation of the above interpretation of LRET data, we have remeasured the distance difference between the fork + RNAP and the duplex using FRET (i.e., using the donor probe with nanosecond rather than microsecond lifetime of the excited state). The 3′ end of the top strand of the fork DNA was labeled with fluorescein, and seven positions within the spacer DNA were labeled with Cy3, an efficient acceptor for fluorescein. Figure 6 shows the examples of donor decay curves which were used to calculate the distances. The pattern of distance differences between the fork−RNAP complex and the duplex (Table 4) was very similar to that observed in LRET experiments [no change in short-range distances (to the sites adjacent to the −10 hexamer) and significantly shorter long-range distances (to the sites adjacent to the −35 hexamer)]. In contrast to LRET experiments, the distances in free fork DNA were similar to the distances in the reference duplex, confirming that unusually short distances in free fork observed with LRET were due to the extensive flexibility of the ss tail.

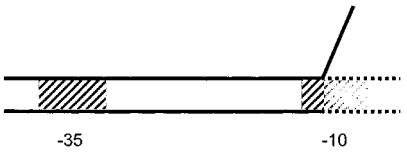

FIGURE 7: Model of the fork DNA conformation when bound to the holoenzyme. The duplex part of the fork was found to be relatively unperturbed by binding to RNAP. A sharp kink at the ds/ss DNA boundary is the simplest interpretation of distance changes observed upon binding to RNAP between the 3′ end of ss nontemplate strand extension and positions in the spacer DNA.

Table 4: Summary of FRET Distance Measurements with the Donor at the 3′ End of the Nontemplate Strand (Position −4)

	distance (Å)			
acceptor position	in full reference duplex	in fork	in fork + holoenzyme	Δ [(fork + holoenzyme)− full duplex] (Å)
−14	45.2	51.2	47.9	+2.7
−16	46.4	48.0	47.1	+0.7
−18	52.3	49.0	48.6	−3.7
−20	53.2			
−22	57.6			
−24	62.8	59.2	52.6	−10.2
−26	65.4	62.0	56.2	−9.2

The characteristic pattern of differences between distances in fork + RNAP and the reference duplex [no change in short-range distances (to the sites adjacent to the −10 hexamer) and significantly shorter long-range distances (to the sites adjacent to the −35 hexamer)] was observed both by LRET and by FRET. The simplest model of the fork DNA bound to RNAP explaining this pattern is shown in Figure 7. Such a pattern can be only obtained if the ss tail is sharply kinked. Other simple deformations (for example, linear contraction of the length of the ss tail) are not consistent with the observed pattern of distance differences between the fork−RNAP complex and the duplex. The angle of the kink was estimated by determining the range of angles which would be consistent within the error of experiment with the range of observed distance differences between the fork−RNAP complex and the reference duplex DNA. The estimated range of the kink angle was between 45° and 90°. The model shown in Figure 7 shows the ss tail at a 67° angle. The exact location of this kink is difficult to pinpoint on the basis of the obtained data. However, taking into account the significant difference in the bendability of ss and ds DNA, it is reasonable to assume that the kink is located at the boundary between ds and ss DNA.

DISCUSSION

Recent years brought significant advances in understanding the structure of multisubunit RNA polymerases. Most significantly, a high-resolution crystal structure of the core enzyme from *T. aquaticus* is now available (*14*). In contrast, the information regarding the conformation of promoter DNA is known only from indirect or low-resolution approaches. The deformation of promoter DNA in complex with polymerase is an important, functional component of the transcription initation reaction. The major change of promoter DNA conformation obviously occurs during open complex formation in which ∼1.5 turns of DNA duplex undergo

melting to ss DNA. In addition, more subtle but possibly important conformational changes of promoter DNA were proposed. DNA bending by RNA polymerase was observed using several techniques (*36*−*39*). Atomic force microscopy measurements predicted wrapping of DNA around the polymerase (*13*). Finally, a distortion of a spacer DNA between the −10 and −35 promoter region upon formation of the initial closed complex was proposed to occur and to function as an energy storage for later use in melting DNA duplex (*5*).

The fork junction DNA studied in this work corresponds to the upstream end of the transcription bubble. The model of DNA conformation in this region built using our LRET measurements reveals a sharp kink of fork junction DNA at the boundary between ss and ds DNA. Thus, our model predicts an abrupt change in DNA trajectory at the boundary of ds and ss DNA at the upstream end of the transcription bubble in the open complex. Such prediction is consistent with a recent model of the open complex developed on the basis of extensive polymerase−promoter DNA cross-linking studies (*40*). Such sharp deformation of DNA required for the efficient interaction of the nontemplate strand in the ss form could be one of the driving forces for DNA melting necessary for the open complex formation. The conformation of the spacer DNA duplex appears to be only slightly perturbed. It will be of interest now to determine the conformation of RNA polymerase-bound promoter DNA in the duplex form corresponding to the closed complex to determine if the sharp DNA kinking observed for the fork junction DNA is functionally coupled to the melting of the DNA duplex. The approaches used in this work to determine the conformation of polymerase-bound fork junction DNA can be extended to address this question.

ACKNOWLEDGMENT

We thank William R. Laws and J. B. Alexander Ross for the software for fluorescence decay data analysis.

REFERENCES

1. Chamberlin, M. (1976) *RNA Polymerase* (Losick, R., and Chamberlin, M., Eds.) pp 17−67, Cold Spring Harbor Laboratory, Cold Spring Harbor, NY.
2. Severinov, K. (2000) *Curr. Opin. Microbiol. 3*, 118−125.
3. Helmann, J. D., and deHaseth, P. L. (1999) *Biochemistry 38*, 5959−5967.
4. Record, M. T., Jr., Reznikoff, W. S., Craig, M. L., McQuade, K. L., and Schlax, P. J. (1996) *Escherichia coli* RNA polymerase ($E\sigma^{70}$), promoters, and the kinetics of the steps of transcription initiation, in *Escherichia coli and Salmonella: cellular and molecular biology* (Neidhardt, F. C., Curtis, R., III, Ingraham, J. L., Lin, E. C. C., Low, K. R., Magasanik, B., Reznikoff, W. S., Riley, M., Schaechter, M., and Umbarger, H. E., Eds.) 2nd ed., pp 792−820, ASM Press, Washington, DC.
5. deHaseth, P. L., and Helmann, J. D. (1995) *Mol. Microbiol. 16*, 817−824.
6. Darst, S. A. (2001) *Curr. Opin. Struct. Biol. 11*, 155−162.
7. Jeon, Y. H., Negishi, T., Shirakawa, M., Yamazaki, M., Fujita, N., Ishihama, A., and Kyogoku, Y. (1995) *Science 270*, 1495−1497.
8. Malhorta, A., Severinova, E., and Darst, S. (1996) *Cell 87*, 127−136.
9. Zhang, G., and Darst, S. (1998) *Science 281*, 262−266.
10. Darst, S. A., Kubalek, E. W., and Kornberg, R. D. (1989) *Nature 340*, 730−732.
11. Polyakov, A., Severinova, E., and Darst, S. A. (1995) *Cell 83*, 365−373.
12. Darst, S. A., Polyakov, A., Richter, C., and Zhang, G. Y. (1998) *J. Struct. Biol. 124*, 115−122.
13. Rivetti, C., Guthold, M., and Bustamante, C. (1999) *EMBO J. 18*, 4464−4475.
14. Zhang, G., Campbell, L., Minakhin, L., Richter, C., Severinov, K., and Darst, S. A. (1999) *Cell 98*, 811−834.
15. Guo, Y., and Gralla, J. D. (1998) *Proc. Natl. Acad. Sci. U.S.A. 95*, 11655−11660.
16. Fenton, M. S., Lee, S. J., and Gralla, J. D. (2000) *EMBO J. 19*, 1130−1137.
17. Matlock, D. M., and Heyduk, T. (2000) *Biochemistry 39*, 12274−12283.
18. Selvin, P. R. (1996) *IEEE J. Sel. Top. Quantum Electron. 2*, 1077−1087.
19. Selvin, P. R., and Hearst, J. E. (1994) *Proc. Natl. Acad. Sci. U.S.A. 91*, 10024−1008.
20. Selvin, P. R., Rana, T. M., and Hearst, J. E. (1994) *J. Am. Chem. Soc. 116*, 6029−6030.
21. Förster, T. (1948) *Ann. Phys. 2*, 55−75.
22. Selvin, P. R. (1995) *Methods Enzymol. 246*, 300−334.
23. Mujumdar, R. B., Ernst, L. A., Mujumdar, S. R., Lewis, C. J., and Waggoner, A. S. (1993) *Bioconjugate Chem. 4*, 105−111.
24. Heyduk, E., and Heyduk, T. (1999) *J. Biol. Chem. 274*, 3315−3322.
25. Burgess, R. R., and Jendrisak, J. J. (1975) *Biochemistry 14*, 4634−4638.
26. Polyakov, A., Severinova, E., and Darst, S. A. (1995) *Cell 83*, 365−373.
27. Hager, D. A., Jin, D. J., and Burgess, R. R. (1990) *Biochemistry 29*, 7890−7894.
28. Heyduk, T., and Lee, J. C. (1990) *Proc. Natl. Acad. Sci. U.S.A. 87*, 1744−1748.
29. Heyduk, E., and Heyduk, T. (1997) *Anal. Biochem. 248*, 216−227.
30. Heyduk, T., and Heyduk, E. (2001) *Anal. Biochem. 289*, 60−67.
31. Lakowicz, J. R. (1999) *Principles of Fluorescence Spectroscopy*, Kluwer Academic/Plenum Press, New York.
32. Grinvald, A., and Steinberg, I. Z. (1974) *Anal. Biochem. 59*, 583−598.
33. O'Connor, D. V., and Phillips, D. (1984) *Time-Correlated Single Photon Counting*, Academic Press, New York.
34. Clegg, R. M., Murchie, A. I., Zechel, A., and Lilley, D. M. (1993) *Proc. Natl. Acad. Sci. U.S.A. 90*, 2994−2998.
35. Norman, D. G., Graigner, R. J., Uhrin, D., and Lilley, D. M. (2000) *Biochemistry 39*, 6317−6324.
36. Heumann, H., Ricchetti, M., and Werel, W. (1988) *EMBO J. 7*, 4379−4381.
37. Kuhnke, G., Theres, C., Fritz, H. J., and Ehring, R. (1989) *EMBO J. 8*, 1247−1255.
38. Meyer-Alme, F. J., Heumann, H., and Porschke, D. (1994) *J. Mol. Biol. 236*, 1−6.
39. Rees, W. A., Keller, R. W., Vesenka, J. P., Yang, G., and Bustamante, C. (1993) *Science 260*, 1646−1649.
40. Naryshkin, N., Revyakin, A., Kim, Y., Mekler, V., and Ebright, R. H. (2000) *Cell 101*, 601−611.

BI012133I